ELSEVIER

Contents lists available at ScienceDirect

Journal of Inorganic Biochemistry

journal homepage: www.elsevier.com/locate/jinorgbio





Metallothionein-3 attenuates the effect of Cu²⁺ ions on actin filaments

Rabina Lakha ^a, Carla Hachicho ^a, Matthew R. Mehlenbacher ^b, Dean E. Wilcox ^b, Rachel N. Austin ^a, Christina L. Vizcarra ^{a,*}

ARTICLE INFO

Keywords:
Metallothionein-3
Actin
Profilin
Cytoskeleton
Copper
Zinc

ABSTRACT

Metallothionein 3 (MT-3) is a cysteine-rich metal-binding protein that is expressed in the mammalian central nervous system and kidney. Various reports have posited a role for MT-3 in regulating the actin cytoskeleton by promoting the assembly of actin filaments. We generated purified, recombinant mouse MT-3 of known metal compositions, either with zinc (Zn), lead (Pb), or copper/zinc (Cu/Zn) bound. None of these forms of MT-3 accelerated actin filament polymerization *in vitro*, either with or without the actin binding protein profilin. Furthermore, using a co-sedimentation assay, we did not observe Zn-bound MT-3 in complex with actin filaments. Cu^{2+} ions on their own induced rapid actin polymerization, an effect that we attribute to filament fragmentation. This effect of Cu^{2+} is reversed by adding either EGTA or Zn-bound MT-3, indicating that either molecule can chelate Cu^{2+} from actin. Altogether, our data indicate that purified recombinant MT-3 does not directly bind actin but it does attenuate the Cu-induced fragmentation of actin filaments.

1. Introduction

Mammalian metallothioneins (MTs) are small (6-8 kDa), cysteinerich proteins that bind seven d^{10} metal ions in two metal-thiolate clusters (Fig. 1; [1]). Their physiological roles include metal detoxification and metal homeostasis, and toward this function MTs interact with both essential (Zn²⁺, Cu⁺) and abiotic (Hg²⁺ and Cd²⁺) metals (reviewed in [2,3]). Among the four mammalian MT isoforms, metallothionein-3 (MT-3) has a distinct expression pattern: it is found predominantly in the central nervous system [4,5] and kidney [6]. Unlike most MTs [7], MT-3 expression is not induced by zinc [8,9] but is upregulated by hypoxia [10–12]. While MT-3 deletion in the mouse has little apparent effect on overall health and cognition, Mt3-null mice do have an enhanced sensitivity to seizures induced by kainate, a neuroexcitatory glutamate analog [13]. Compared to wild type mice, Mt3-null mice have similar levels of copper in the brain but less zinc in certain brain regions, including the hippocampus [13]. To our knowledge, kidney function and metal concentrations have not been studied in the Mt3-null mice.

MT-3 has a unique biological activity: it inhibits brain extracts from promoting the survival of cultured neurons [14], an activity that is not shared by other MT isoforms [15,16]. In fact, the *Mt3* gene product was initially named growth inhibitory factor (GIF) before it was renamed when molecular cloning revealed its homology to canonical MTs [4,17].

While brain extracts from both Alzheimer's disease (AD) patients and aged-matched controls are neurotrophic, the AD brain extract is approximately two-fold more potent than control extracts at promoting survival of cultured neurons [14,15]. Some have attributed this difference to lower levels of MT-3 in AD brain extracts [17,18], while others have found that MT-3 levels are unchanged in AD [15,19]. A molecular mechanism of growth inhibition by MT-3 has not been elucidated. However, the domain and MT-3-specific sequence motifs that are essential for GIF activity have been mapped. MT-3's N-terminal β domain is necessary for growth inhibition [16,20]. The C-terminal α domain may be dispensable for GIF activity [16], or it may stabilize the β domain by domain-domain interactions [21]. Mutational studies identified two conserved prolines (Pro7 and Pro9) and a threonine (Thr5) that are unique to MT-3 as essential for GIF activity [16,22,23]. Since the growth inhibition bioassay reflects MT-3's attenuation of brain extract-induced growth stimulation [15,16], it is likely that MT-3 interacts specifically with some component of the extract or with a neuronal receptor.

Motivated by the potential importance of protein-protein interactions in MT-3 function, several screens have been carried out to characterize MT-3's interactome [24–26]. Using immunoaffinity chromatography and tandem mass spectrometry, at least 12 proteins have been identified that bind to MT-3 [24,25]. Of particular interest to this

E-mail address: cvizcarr@barnard.edu (C.L. Vizcarra).

^a Department of Chemistry, Barnard College, New York, NY 10027, USA

^b Department of Chemistry, Dartmouth College, Hanover, NH 03755, USA

^{*} Corresponding author.

work, the cytoskeletal protein actin (β and γ isoforms) was one of the proteins most often identified in complex with MT-3 in these screening studies [24–26]. Based on the list of MT-3-binding proteins, Armitage and coworkers proposed that MT-3 is secreted from astrocytes through its interaction with Rab3A, Exo84p, and 14–3-3 zeta and then transported into neurons through interaction with plasminogen (PGn) and enolase, where MT-3 could inhibit growth through its effect on the cytoskeleton and/or other interactions [25].

In addition to the appearance of actin in interaction screens, MT-3 and actin have been functionally linked in mouse astrocytes [27,28] and in human kidney proximal tubule cells [26]. In astrocytes, changes in the actin cytoskeleton that occur downstream of epidermal growth factor (EGF) treatment are abnormal in the absence of MT-3 [27]. In the same study, two observations supported a direct binding interaction between MT-3 and actin. First, GFP-MT-3 was detected in the pellet fraction after high-speed centrifugation of astrocyte lysates, consistent with an interaction between GFP-MT-3 and actin filaments ('F-actin'). Second, GFP-MT-3 isolated from astrocytes enhanced actin polymerization in an *in vitro* pyrene-actin polymerization assay [27]. Addition of the zinc chelator TPEN blocked MT-3-induced actin polymerization, while the addition of Zn-bound TPEN did not, suggesting that MT-3 must be in a Zn-bound and not a Cu-bound state to accelerate actin assembly [27].

The connection between Zn and MT-3-induced actin polymerization [27] is surprising because the β domain of MT-3 isolated from brain is Cu-bound [29], giving an overall metal stoichiometry of Cu₄Zn_{3.4}MT-3 [17]. Furthermore, MT-3 is the most copper-philic of the mammalian MTs [30,31]. In general, copper is an essential and highly regulated trace element with a variety of roles in normal growth, development, and cellular metabolism [32] and is known to bind to both actin [33] and MT-3 [31,34]. In hippocampal neurons, copper is enriched in dendrites compared to somata, where nano X-ray fluorescence suggests it co-localizes with actin filaments in dendritic spine necks [35]. Both copper supplementation with added CuSO₄ and copper chelation by neocuproine resulted in decreased actin filament content in dendrites [35], suggesting that Cu levels impact the actin cytoskeleton. In vitro, it was found that Cu²⁺ binds with subpicomolar affinity to monomeric actin through Cys374, an interaction that still allows actin to polymerize into filaments [33]. Electron microscopy studies showed that Cu²⁺ ions induce fragmentation of actin filaments, leading to shorter filaments but not complete depolymerization [36]. The Cu-binding properties of MT-3 have been linked to its neuronal protective abilities: MT-3 can swap its

bound Zn^{2+} for Cu^{2+} that is bound to neurologically important peptides like amyloid- β peptides, α -synuclein, and prion protein, reducing Cu^{2+} to Cu^{+} through formation of disulfide bonds and thereby eliminating harmful redox chemistry associated with copper [37–40].

Despite evidence for an interaction between actin and MT-3, it is unclear whether they bind directly or their interaction is mediated by other proteins, metal ions, and/or post-translational modification. If actin and MT-3 do form a stable protein-protein complex, it is unknown whether this is critical to MT3's GIF activity and potential neuro-protective roles. MT-3's role as a metal chelator and metal chaperone suggest other mechanisms by which MT-3 and actin might impact each other's functions. Careful biochemical characterization of the MT-3-actin interaction is required to better understand the role of MT-3 in the central nervous system. Such characterization must consider the different potential metalation states of MT-3, as well as the possibility of *in vivo* phosphorylation in mammalian systems. In this study, we show that while purified recombinantly-expressed MT-3 has minimal direct effect on actin filament dynamics, MT-3 modulates the effect of Cu²⁺ on actin filaments.

2. Methods

Mouse MT-3 (UniProt P28184) was expressed in BL21-DE3-pLysS E. coli cells and purified as previously described [34]. To produce different metalation states (Zn₇MT-3, Pb₇MT-3, Cu₄Zn₄MT-3), stock solutions of either ZnCl2, Pb(NO3)2, and/or CuCl2 were added to apo-MT-3 (in 100 mM MES, 150 mM NaCl, pH 6.4) in stoichiometric amounts inside an anaerobic Coy glovebox with a 95% N2 and 5% H2 environment. A non-GIF mutant (Pro7Ser/Pro9Ala) and a phosphomimetic mutant (Ser33Asp) were both constructed by PCR-based mutagenesis [41] (DNA sequences in SI) and purified using the same protocol as WT MT-3 [34]. Using these and similar protocols, we have obtained samples with binding stoichiometries, determined by isothermal titration calorimetry (ITC), that are consistent with Zn₇MT-3 [34,42] and Pb₇MT-3 [42]. Because the mixed Cu/Zn state of MT-3 was created using Cu²⁺, we expect that two disulfide bonds formed per MT-3, concomitant with Cu_4^{1+} cluster assembly in the β domain, as described previously [38,43].

Rabbit skeletal muscle actin from acetone powder (*Pel-Freez Bi-ologicals*) and recombinant *S. pombe* profilin were purified, and actin was labeled as previously described [44].

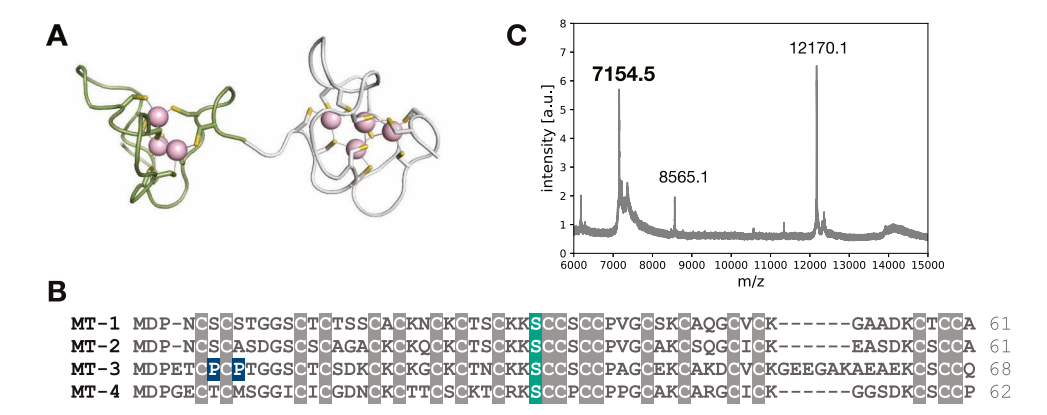


Fig. 1. Structure and sequence alignment of metallothioneins (MTs). (A) The solution structure of MT-2 is shown with cadmium bound. The N-terminal β -domain (green; 2MHU) and the C-terminal α -domain (gray;1MHU) have three and four Cd²⁺ ions bound, respectively. (B) The four mouse metallothioneins were aligned using accession numbers: NP_038630.1 (MT-1), NP_032656.1 (MT-2), NP_038631.1 (MT-3) and NP_032657.1 (MT-4). Cysteine residues are highlighted in gray. The two mutated prolines in the non-GIF P7S/P9A mutant are highlighted in blue, and the serine mutated in the S33D mutant is highlighted in green. The numbers on the right of the sequence indicate the number of amino acids in each MT. (C) MALDI of the purified MT-3 showing the molecular weight at 7154.5 Da. The predicted molecular weight is 7153.3. The other two masses are from calibration buffer. (For interpretation of the references to colour in this figure legend, the reader is referred to the web version of this article.)

2.1. Fascin purification

Human fascin-1 protein was expressed in BL21-DE3* E. coli cells. Terrific broth (1 L supplemented with 100 µg/mL ampicillin) was inoculated with 10 mL of dense culture grown for 16 h at 37 °C. These large cultures were shaken at 250 rpm and 37 °C until the cells reached the optical density of 0.3-0.6 at 600 nm. The cultures were then cooled to 18 °C for 30 min, and protein expression was induced with 0.25 mM isopropyl β-D-1-thiogalactopyranoside (IPTG). The cells were harvested by centrifugation, resuspended in PBS (140 mM NaCl, 2.7 mM KCl, 10 mM Na₂HPO₄, and 1.8 mM KH₂PO₄ pH 7.3), flash frozen in liquid nitrogen, and stored at $-80~^{\circ}$ C. To isolate fascin protein, 20 g of frozen cells were thawed and brought to 30 mL with lysis buffer (50 mM Tris-HCl, 500 mM NaCl, pH 8.0) supplemented with 1 mM phenylmethylsulfonyl fluoride (PMSF), 1 mM dithiothreitol (DTT) and 4 µg/mL DNase (Sigma catalog no. DN25). Cells were lysed using a French press and the lysate was centrifuged at 30,000 $\times g$ for 30 min. The supernatant was nutated with 2 mL glutathione Sepharose resin slurry (Cytiva) for 1 h. The slurry was poured into a column and the resin was washed first with the lysis buffer followed by a low salt buffer (50 mM Tris-HCl, 100 mM NaCl, 1 mM DTT, pH 8.0). Protein was then eluted with glutathione elution buffer (50 mM Tris-HCl, 100 mM NaCl, 100 mM glutathione, 1 mM DTT, pH 8.0) and dialyzed into low salt buffer at 4 °C overnight. His6-tagged TEV protease (purified as described [34]) was added to the protein in dialysis tubing to cleave the fusion protein. The sample was nutated with glutathione Sepharose for 1 h to separate the cleaved fascin from GST. The unbound protein was collected and nutated with Ni-NTA resin for 1 h. The unbound fraction was collected from the Ni-NTA column and dialyzed into KMEI dialysis buffer (50 mM KCl, 1 mM EGTA, 1 mM $MgCl_2$, 10 mM imidazole, 1 mM DTT, pH 7.0) overnight. The protein was concentrated using the Amicon 30 kDa centrifugal filter, and the final concentration was measured using an extinction coefficient of 68,465 M⁻¹ cm⁻¹ at 280 nm. Proteins were aliquoted in small fractions, flash-frozen in liquid nitrogen, and stored at $-80\,^{\circ}$ C.

2.2. MALDI-TOF mass spectrometry

Matrix-assisted laser desorption ionization time of flight (MALDITOF) mass spectrometry was carried out using a Bruker ultrafleXtreme MALDI TOF/TOF instrument fitted with a frequency-tripled Nd:YAG laser (355 nm). The matrix contained 10 mg/mL sinapinic acid in 70:30 water:acetonitrile with 0.1% trifluoroacetic acid. Each protein sample was prepared in the ratio of 3:7 protein:matrix, and 1 μ L of that mixture was spotted onto a stainless steel sample plate followed by drying at room temperature. The data were collected in linear positive-ion mode.

2.3. Actin co-sedimentation and monobromobimane labeling

Actin co-sedimentation assays were performed to test for an interaction between Zn₇MT-3 and F-actin. Monomeric actin was first polymerized by adding KMH polymerization buffer (1× concentrations: 50 mM KCl, 1 mM MgCl₂, 10 mM HEPES, pH 7) and incubating at room temperature for 30 min. The F-actin was then incubated with either a range of Zn₇MT-3 concentrations (20, 10, 5 and 2.5 μ M) or fascin (5 μ M) for 1 h at room temperature. The samples were then centrifuged at $100,000 \times g$ at 4 °C for 90 min. The supernatants were removed, and the pellets were resuspended in monobromobimane (mBrB) labeling buffer (60 mM Tris-Cl, 20 mM EDTA, 20 mM TCEP, pH 8.0) [45]. Equal volumes of mBrB labeling buffer and supernatant were mixed. A stock solution of 100 mM mBrB dye in acetonitrile was added to each sample to reach a final mBrB concentration of 12.5 mM. The samples were then incubated at room temperature in the dark for 1 h. Excess mBrB was removed by extraction into methylene chloride. The samples were analyzed by SDS-PAGE (Bio-Rad AnyKD gel, 160 V, 45 min) and Coomassie stained.

2.4. Actin assembly assays

Bulk actin assembly assays were carried out as described [44], with a few changes. EGTA was excluded from the polymerization assays to avoid metal chelation. The polymerization buffer used was KMH (50 mM KCl, 1 mM MgCl₂, 10 mM HEPES, pH 7.0) with 0.2 mM ATP. For the assays shown in Fig. S1, 10 mM MOPS was used in place of HEPES. In specific cases, EGTA, CuCl₂, and/or ZnCl₂ was added to the assay as indicated. Fluorescence was monitored at 15-s intervals using a TECAN F200 plate reader with an excitation filter at 360 nm (35 nm bandwidth) and an emission filter of 415 nm (20 nm bandwidth). The polymerization rate at a time of interest is the slope of a best-fit line to either 3 or 15 data points (4 µM actin or 3 µM actin/6 µM profilin traces, respectively) centered at the time of interest (Figs. 5 and S4). To collect the images in Fig. 2C, $\approx 10 \,\mu\text{L}$ of reaction mixture was removed from the pyrene-actin polymerization assay at 50 s and 1500 s. These samples were mixed with Acti-stain488 phalloidin (Cytoskeleton, Inc.) at an equimolar actin to phalloidin ratio, diluted 50-fold into imaging buffer ($1 \times$ KMH, 5 mM DTT), and immobilized on poly-L-lysine coated coverslips. Imaging conditions are described below. For pyrene assays, each condition was measured with at least three replicates collected over at least two separate days. For MT-3 titrations (Figs. 5 and S4), polymerization rates for replicates are plotted. For CuCl2 and ATP titrations, traces that are representative of three replicates are shown.

2.5. ICP mass spectrometry

After the co-sedimentation assay, separated supernatants and pellets were mixed with equal volumes of 68% trace metal grade $\rm HNO_3$ overnight. The digested samples were diluted 400-fold by adding 10 mL of milliQ water. Samples were analyzed on a Multi-element ICP-MS (Element XR). The mass percentage of Cu in the pellet was calculated using the ppb of the pellet fraction, obtained from ICP-MS, divided by the total ppb of the pellet and the supernatant, multiplied by 100.

2.6. Fluorescence microscopy

Monomeric actin was polymerized to form F-actin for 30 min at room temperature in $1 \times$ KMH. Samples were prepared at room temperature by incubating 5 μM F-actin with 5 μM Cu²⁺ as indicated for 10 min, followed by addition of 5 μM EGTA or 5 μM Zn₇MT-3. After a 5-min incubation time, each sample was labeled with 2:1 Acti-stain488 phalloidin:actin, and further diluted by adding 1900 µL of imaging buffer to reach the final concentration of 6.5 nM F-actin and 12.5 nM phalloidin. Slides were prepared from each sample by pipetting 10 µL of sample onto a poly-L-lysine-coated coverslip. Samples were visualized using a Nikon Ti2 inverted microscope equipped with a TI-LA-HTIRF module and an ORCA-Flash 4.0 LT+ sCMOS camera, controlled with NIS-Elements software. An apochromat TIRF 100 × oil-immersion objective lens (N.A. 1.49) was used with a 400 ms exposure time and 2% (Fig. 2) or 5% (Fig. 3) power with a 20-mW 488 nm argon laser. All image analysis was conducted using the FIJI distribution of the ImageJ software [46]. Filament lengths were measured manually by creating snakes in the JFilament plugin [47,48].

2.7. Isothermal titration calorimetry

 $\rm Zn_7MT$ -3 samples in 100 mM BisTris, 150 mM NaCl, pH 7.4 were stored and sample preparation occurred within a Coy Laboratory glovebox that maintains a $\rm N_2$ environment, with daily addition of $\rm H_2$. A platinum catalyst, which reacts with trace $\rm O_2$, and the $\rm H_2$, to form water, maintains low ppm oxygen. All buffers were made metal-free by soaking with Chelex resin ($\rm Sigma$), filtered, and thoroughly degassed under vacuum before transfer into the glovebox. Diethylenetriaminepentaacetic acid (DTPA) was weighed into a borosilicate glass vial and brought into the glovebox for dissolution in deoxygenated buffer. The

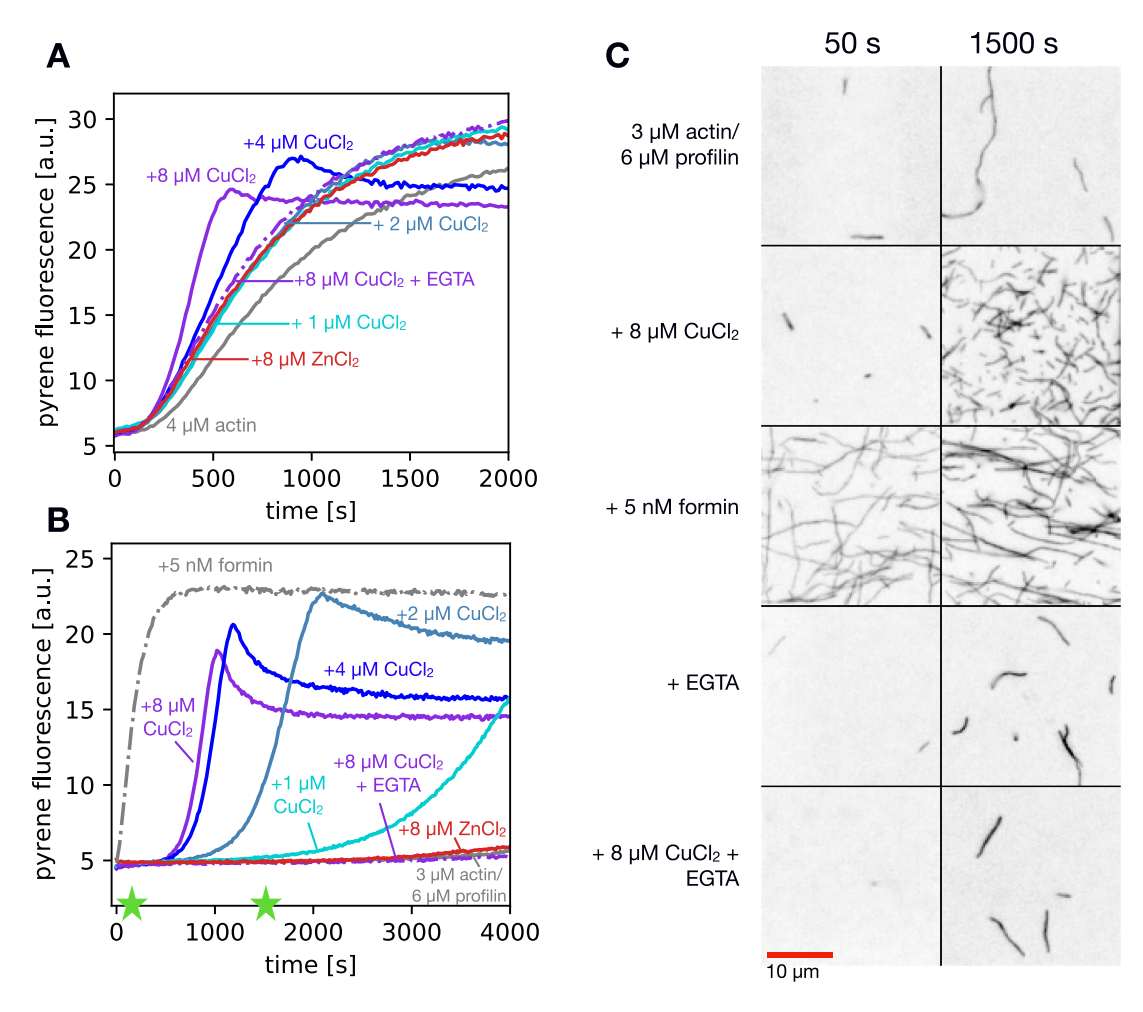


Fig. 2. Effects of copper on actin polymerization. Pyrene-actin polymerization was measured in the presence of $CuCl_2$, $ZnCl_2$ and/or EGTA with (A) 4 μ M actin or (B) 3 μ M actin and 6 μ M profilin. In all experiments, 5% of actin monomers were pyrene-labeled. In the presence of copper ions, a rapid increase in pyrene signal was observed after an initial lag period. This effect was particularly pronounced in the presence of profilin. The chelator EGTA (1 mM) reversed the effect of $CuCl_2$ on actin polymerization. A replicate of the conditions with $CuCl_2$ and $ZnCl_2$ is shown in Fig. S5. (C) Actin filaments were imaged using TIRF microscopy, sampled at two time points in the profilin/actin polymerization reaction. The green stars indicate the times (50 s and 1500 s) when a small amount of actin was removed from the assay and mixed with equimolar Acti-stain488 phalloidin, diluted 50×10^{-5} into imaging buffer, and immobilized on poly-L-lysine coated coverglass. (For interpretation of the references to colour in this figure legend, the reader is referred to the web version of this article.)

DTPA concentration was confirmed with ITC by titration with a known concentration of Zn^{2+} . The experimental stoichiometry and binding enthalpy were compared to known values.

All ITC experiments were completed with a Malvern Panalytical (MicroCal) VP-ITC, which is housed in a custom-built glovebox that is purged with N_2 to ensure an anaerobic environment. The ITC measurements used injection volumes of 4 or 5 μL , a stir speed of 307 rpm and a temperature set at 25 \pm 0.2 °C. The heat of the final injections, after binding was complete, was used as the heat of dilution and subtracted from each data point. The isotherms were analyzed with Origin Pro data analysis software using a one-site fitting model, which uses a least-square fitting equation. Titrations of DTPA into S33D Zn_7MT-3 were repeated four times and the reported errors are the standard deviations for the measurements.

3. Results

Given the potential importance of the MT-3-actin interaction in explaining the unique biological function of MT-3, we thought it important to characterize how actin polymerization is affected by purified MT-3, without a large GFP tag and in well-defined metalation states. The polymerization of actin monomers into filaments is critical to

the function of actin, and this transition from monomer to filaments was proposed as the step at which MT-3 regulates the actin cytoskeleton in astrocytes [27].

3.1. Copper ions alter actin filament morphology

Before testing the effect of MT-3 on actin polymerization, we first tested the effect of relevant divalent metal ions in the pyrene-actin polymerization assay. The pyrene assay allows real-time monitoring of the transition from monomeric actin to filamentous actin using the increase in fluorescence of pyrene-labeled actin upon its incorporation into the filament [49,50]. In our experiments, 5% of the actin monomers were pyrene-labeled at residue Cys374, and the remaining 95% were unlabeled. We measured pyrene-actin fluorescence over time in the presence of Zn²⁺ and Cu²⁺, both with and without the actin-binding protein profilin, which is present at high concentration in non-muscle cells and suppresses spontaneous actin filament nucleation (reviewed in [51]). In our experiments, Cu^{2+} addition caused rapid polymerization after a long lag period, an effect that was not observed when Zn²⁺ was added (Fig. 2A). The Cu²⁺-induced increase in the polymerization rate was more prominent in the presence of profilin (Fig. 2B). Our standard polymerization solution contains HEPES buffer, which can be oxidized

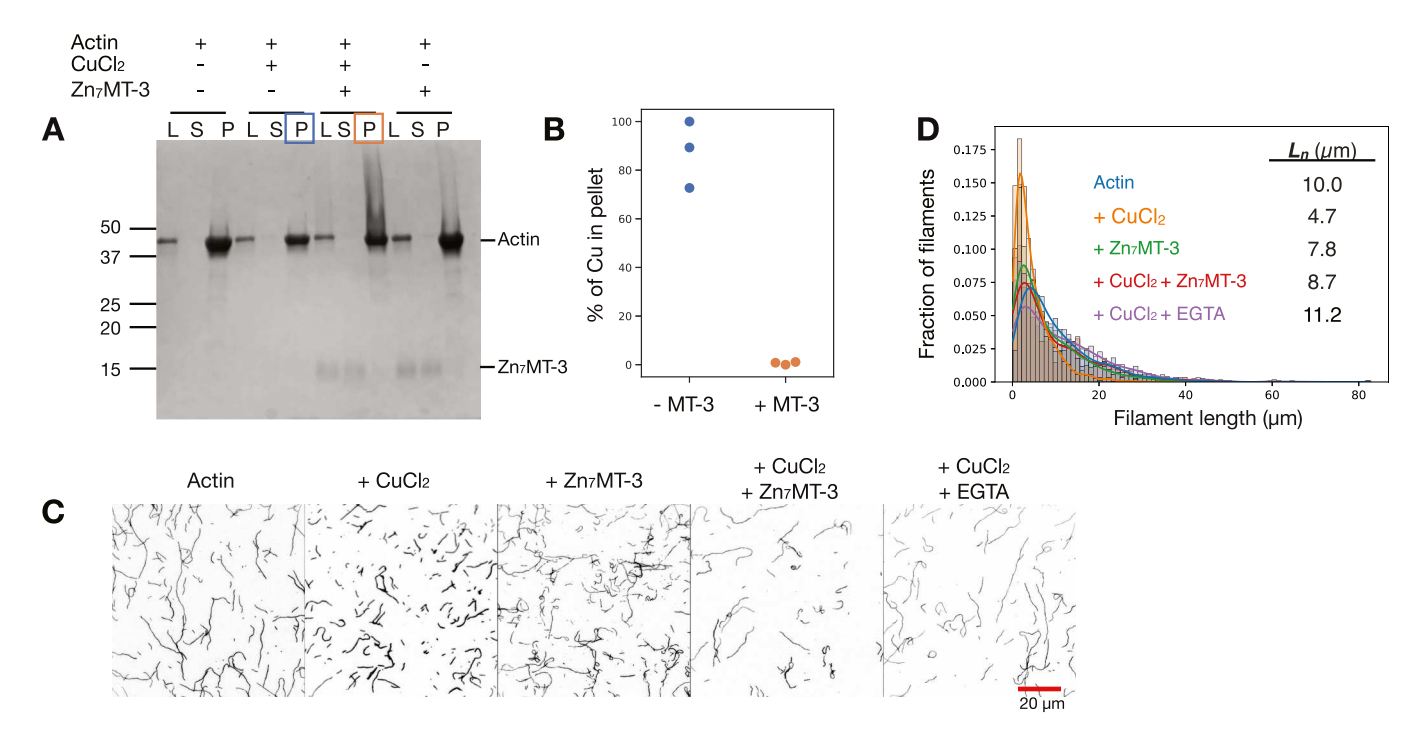


Fig. 3. Copper ions induce actin filament fragmentation and MT-3 reverses it. (A) Co-sedimentation assay of 5 μM F-actin with CuCl₂ (5 μM) and/or Zn₇MT-3 (5 μM). After separating supernatant (S) and pellet (P) fractions, samples were labeled with monobromobimane, separated by SDS-PAGE, and stained with Coomassie. Under these conditions, there is no detectable Zn₇MT-3 in the pellet. The pellets were concentrated 4-fold compared to the load (L) and supernatants. (B) ICP-MS quantification of the amount of copper ions in pellet (P) in the presence and absence of Zn₇MT-3. Pellets boxed with blue and orange in panel A were analyzed in panel B. (C) Actin filaments were imaged using TIRF microscopy in the presence of different combinations of CuCl₂, Zn₇MT-3, and EGTA. All samples were mixed with Acti-stain488 phalloidin, before 50-fold dilution into imaging buffer and immobilization on poly-Lysine coated coverglass. Actin filaments appeared fragmented when exposed to CuCl₂. This effect was reversed with the addition of Zn₇MT-3 or EGTA. (D) Histogram of filament lengths for each condition along with the average length (L_n). The numbers of filaments counted for each condition were 1175 (Actin only), 1626 (+ CuCl₂), 808 (+ Zn₇MT-3), 541 (+ CuCl₂ + Zn₇MT-3), and 897 (+ CuCl₂ + EGTA). A replicate of this experiment with completely different protein preparations is shown in Fig. S6. (For interpretation of the references to colour in this figure legend, the reader is referred to the web version of this article.)

by Cu^{2+} to form insoluble Cu^{+} species [52–54]. Therefore, we repeated the profilin/actin polymerization assay using MOPS (Fig. S1), a buffer that does not react with Cu^{2+} [53]. The effect of Cu^{2+} on polymerization kinetics was similar in MOPS (Fig. S1) and HEPES (Fig. 2B), indicating that Cu^{2+} -induced acceleration of actin polymerization is not an artifact of the unique redox chemistry between Cu^{2+} and HEPES. The effect of Cu^{2+} on actin filaments was suppressed by the addition of 1 mM EGTA in the polymerization buffer (Fig. 2A,B, dashed purple lines).

The pyrene assay is a bulk measurement that provides only the total concentration of monomer in the polymer form but does not provide information about the length distribution of the filaments. We observed a long lag time before the acceleration of actin polymerization over baseline rates, which is consistent with Cu²⁺ ions causing fragmentation of spontaneously-nucleated actin filaments. Fragmentation would create more barbed ends and thus increase the rate of filament growth [55]. To test this model, actin filaments were imaged using TIRF microscopy at two different points in the time course of polymerization (marked by stars in Fig. 2B). The addition of Cu²⁺ ions induced short filaments (Fig. 2C), consistent with electron microscopy of Cu-treated actin filaments [36]. These filaments were notably shorter than those observed in the presence of the formin DIAPH2, one of the human Diaphanousrelated formins, which generally accelerate both actin filament nucleation and elongation in the presence of profilin [56]. The effect of Cu²⁺ ions on filament length was reversed by adding EGTA (Fig. 2C). Taken together, the kinetics observed in the pyrene-actin assays (Fig. 2A-B) and the short filament lengths observed by microscopy are consistent with filament fragmentation by Cu2+ ions. Spectroscopic data also indicate that Cu²⁺ binding affects intermolecular interactions within the actin filament [57].

3.2. MT-3 reverses the effect of copper ions on actin filament morphology

We next tested whether MT-3 could reverse the effects of Cu²⁺ on actin filament length. In reconstituted systems, MT-3 scavenges Cu²⁺ from pathological protein aggregates such as amyloid β -peptides and α -synuclein [37,39]. First, we tested whether, under our assay conditions, Zn₇MT-3 forms a stable complex with actin filaments. We used high-speed co-sedimentation and SDS-PAGE with monobromobimane modification. Under standard, reducing SDS-PAGE conditions, MT-3 runs on the gel anomalously as a diffuse band and is poorly stained by Coomassie, presumably due to its hydrophilicity and lack of aromatic residues. Monobromobimane is a thiol-reactive dye that increases the hydrophobicity of MT-3 and allows detection by Coomassie staining [45]. As expected, actin is present in the pellet fraction after high-speed centrifugation, even in the presence of Cu²⁺, indicating that short filaments are sedimented under these conditions (Fig. 3A). While our pyrene-actin data (Fig. 2A) indicate an ≈11% decrease in steady state Factin in the presence of equimolar Cu²⁺, we see minimal actin in the supernatant when F-actin is exposed to CuCl₂ (Fig. 3A). A more sensitive gel staining technique would be required to quantify small changes in steady state actin after high-speed pelleting. When equimolar actin and Zn₇MT-3 were mixed, Zn₇MT-3 was detected in the supernatant fraction in both the presence and absence of Cu²⁺ ions (Fig. 3A; see below for a wider concentration range of Zn₇MT-3).

To track the binding partner for copper in our co-sedimentation assays, we analyzed the supernatant and pellet fractions using inductively coupled plasma mass spectrometry (ICP-MS). In the absence of $\rm Zn_7MT$ -3, at least 75% of the detected copper was in the pellet fraction (blue markers in Fig. 3B), consistent with $\rm Cu^{2+}$ bound tightly to actin filaments and therefore co-sedimenting with actin. In the presence of

 Zn_7MT -3, less than 2% of the detected copper was in the pellet fraction (blue markers in Fig. 3B), suggesting a transfer of copper from actin filaments to soluble Zn_7MT -3.

We next asked whether the Cu^{2^+} -induced fragmentation that we had observed by microscopy (Fig. 2C) could be reversed by the addition of $\text{Zn}_7\text{MT-3}$. In these experiments, F-actin was mixed with Cu^{2^+} for 10 min before addition of either $\text{Zn}_7\text{MT-3}$ or EGTA. Quantification of actin filament lengths showed that the presence of $\text{Zn}_7\text{MT-3}$ had a modest effect on filament length: $10.0~\mu\text{m}$ vs 7.8 μm average length without and with $\text{Zn}_7\text{MT-3}$, respectively (Fig. 3C,D). With exposure to only Cu^{2^+} , short filaments were observed (4.7 μm ; Fig. 3C,D). Addition of either $\text{Zn}_7\text{MT-3}$ or EGTA, to the Cu^{2^+} -fragmented actin resulted in longer actin filaments, presumably through re-annealing [58] following chelation of the Cu^{2^+} (Fig. 3C,D). Altogether, the data in Fig. 3 are consistent with the transfer of copper ions from F-actin to $\text{Zn}_7\text{MT-3}$ in a mechanism that does not involve a stable MT-3-F-actin complex, similar to other metal swap reactions that have been reported for MT-3 [59].

3.3. Recombinant MT-3 does not bind actin filaments or accelerate actin polymerization

Based on a report that GFP-MT-3 co-sediments with F-actin in astrocyte lysates [27], we were surprised to see minimal co-sedimentation of Zn₇MT-3 and F-actin (Fig. 3A). To further explore this putative binding interaction, we carried out a co-sedimentation assay using an extended range of Zn₇MT-3 concentrations (from 0.5:1 to 4:1 Zn₇MT-3:actin). At all concentrations tested, Zn₇MT-3 was detected only in the supernatant (Fig. 4). A known actin-bundling protein, fascin, was used as a positive control and was detected in the pellet in the presence of F-actin (Fig. 4). From these data, we conclude that either purified, recombinant Zn₇MT-3 does not form a stable complex with F-actin, or, if it does form a complex, the equilibrium dissociation constant (K_d) is much greater than 20 μ M and outside the limit of detection for this assay.

Next, we tested the effect of MT-3 on actin polymerization kinetics using the pyrene-actin polymerization assay, both with and without profilin. For this assay, we prepared MT-3 in three metalation states: Zn₇MT-3 since this form was reported to interact with actin [27], Cu₄Zn₄MT-3 to mimic the physiological form of MT-3 [17,29], and Pb₇MT-3 since Pb²⁺ can displace Zn²⁺ bound to MT-3 [42] and therefore may be bound to MT-3 *in vivo* following lead exposure. No change in the actin polymerization rate was observed at any concentration of MT-3, in any metalation state (Fig. 5). Representative traces are shown in panels 5A, B, D, E, G, and H, and replicates for each condition are shown in

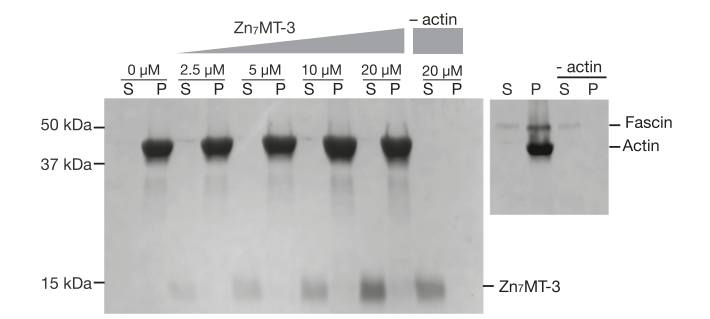


Fig. 4. Co-sedimentation assay with Zn_7MT -3 and F-actin. Zn_7MT -3 (0, 2.5, 5, 10, or 20 μ M) was incubated with 5 μ M F-actin and then centrifuged at 90,000 $\times g$ for 90 min. The presence of Zn_7MT -3 in supernatant (S) and actin in pellet (P) implies either (1) that there is not a direct Zn_7MT -3/F-actin interaction or (2) that the complex has a dissociation constant (K_d) much greater than 20 μ M. Fascin (5 μ M) was used as control protein which binds to F-actin (right image). Samples were labeled with monobromobimane, separated by SDS-PAGE, and Coomassie stained. The pellets were concentrated 4-fold compared to the supernatants.

panels 5C, F, and I. As a positive control, we added 5 nM of the formin DIAPH2 to demonstrate that the profilin-actin was competent for polymerization (panels 5B, E and H). These data are different from the report that astrocyte-derived GFP-MT-3 increased the pyrene-actin signal by $\approx 30\%$, indicative of an increase in the steady-state concentration of F-actin [27] (see below for further discussion).

The pyrene-actin polymerization assays in Fig. 5 were carried out at in the presence of 0.2 mM ATP, which binds MT-2 with a $\rm K_d$ of 176 μM and causes large-scale structural changes in MT-2 [60]. We reasoned that ATP in our polymerization assays may affect the MT-3-induced acceleration of actin polymerization, either promoting or inhibiting MT-3-actin interactions. Therefore, we varied the concentration of ATP from 0.01 to 1 mM. Zn₇MT-3 did not accelerate the rate of actin polymerization at any ATP concentration (Fig. S2). While we cannot rule out an MT-3-ATP interaction, if there is any ATP binding, it does not affect MT-3-actin interactions in the range of concentrations tested (0.01–1 mM).

The difference in actin regulation between our recombinant, bacterially expressed MT-3 (Fig. 5) and astrocyte-derived GFP-MT-3 [27], led us to speculate that recombinant MT-3 was missing a crucial posttranslational modification that is important for its interaction with the actin cytoskeleton. To our knowledge, the only reported posttranslational modification of metallothionein is phosphorylation of MT-1 at serine 32 (Ser33 in MT-3) [61]. This site is phosphorylated by protein kinase C in response to sub-lethal, pre-conditioning stimuli in cultured neurons. This event has been linked to an increased cytosolic concentration of Zn²⁺ [61], suggesting that this Ser32/33 modification may lower the affinity of metallothionein for Zn²⁺. We created a phospho-mimetic version of MT-3 with the mutation Ser33Asp (S33D). First, we measured the affinity of S33D MT-3 for Zn²⁺ using a wellestablished isothermal titration calorimetry (ITC) chelation assay [34]. From these experiments, we determined the Zn²⁺ binding free energy, $\Delta G^{\circ}_{ITC.S33D} = -10.1 \pm 0.3 \text{ kcal} \bullet \text{mol}^{-1}$ (Fig. S3), for comparison to that of WT MT-3, $\Delta G^{\circ}_{ITC,WT} = -9.5 \pm 0.4 \text{ kcal} \cdot \text{mol}^{-1}$ [34], which give similar binding constants of $\textit{K}_{\textit{ITC},\textit{S33D}} = 3~(\pm~1) \times 10^7$ and $\textit{K}_{\textit{ITC},\textit{WT}} = 1.1$ $(\pm 0.9) \times 10^7$. Surprisingly, the enthalpic contribution to Zn^{2+} binding (ΔH°_{ITC}) is $\approx 2 \text{ kcal} \cdot \text{mol}^{-1}$ more favorable for WT than for S33D. This difference is compensated for by an entropic contribution to Zn²⁺ binding $(-T\Delta S^{\circ}_{ITC})$ at 25 °C that is \approx 2.5 kcal•mol⁻¹ more favorable for S33D than for WT, leading to similar overall binding affinities (Fig. S3B). The Zn:MT-3 binding stoichiometries were also similar for WT (6.5 \pm 0.1 Zn:MT3) and S33D MT-3 (7.4 \pm 0.2), supporting our assignment of S33D Zn₇MT-3. In pyrene-actin polymerization assays, S33D Zn₇MT-3, like WT Zn₇MT-3, did not alter the kinetics of actin polymerization (Fig. S4D-F). Mutating the two N-terminal prolines that are unique to MT-3 alters the structure and dynamics of the β domain and abolishes GIF activity [16] but does not alter zinc binding affinity [22]. We therefore tested whether a non-GIF mutant of MT-3 (P7S/P9A Zn₇MT-3) would have distinct interactions with the cytoskeleton. In pyrene-actin polymerization assays, this variant behaved similar to WT Zn₇MT-3, with no effect on actin polymerization (Fig. S4A-C).

4. Discussion

Actin and MT-3 have been linked in a number of studies [24–28]. These links motivated us to investigate the molecular properties underlying the actin-MT-3 interaction and to probe the role of metal ions in this interaction. Overall, our results suggest that recombinant MT-3 and actin do not bind directly. However, due to the fact that they share a common binding partner in copper ions, MT-3 and actin modulate each other's properties. This is most evident in our experiments that monitored length distribution of actin filaments in the presence of Cu^{2+} , with or without $\mathrm{Zn_7MT-3}$ (Fig. 2). Electron paramagnetic resonance indicates that copper ions bound to actin are in the +2 oxidation state [33]. While it is clear from our microscopy data that the effect of Cu^{2+} on actin filament morphology is altered by $\mathrm{Zn_7MT-3}$, we also presume that

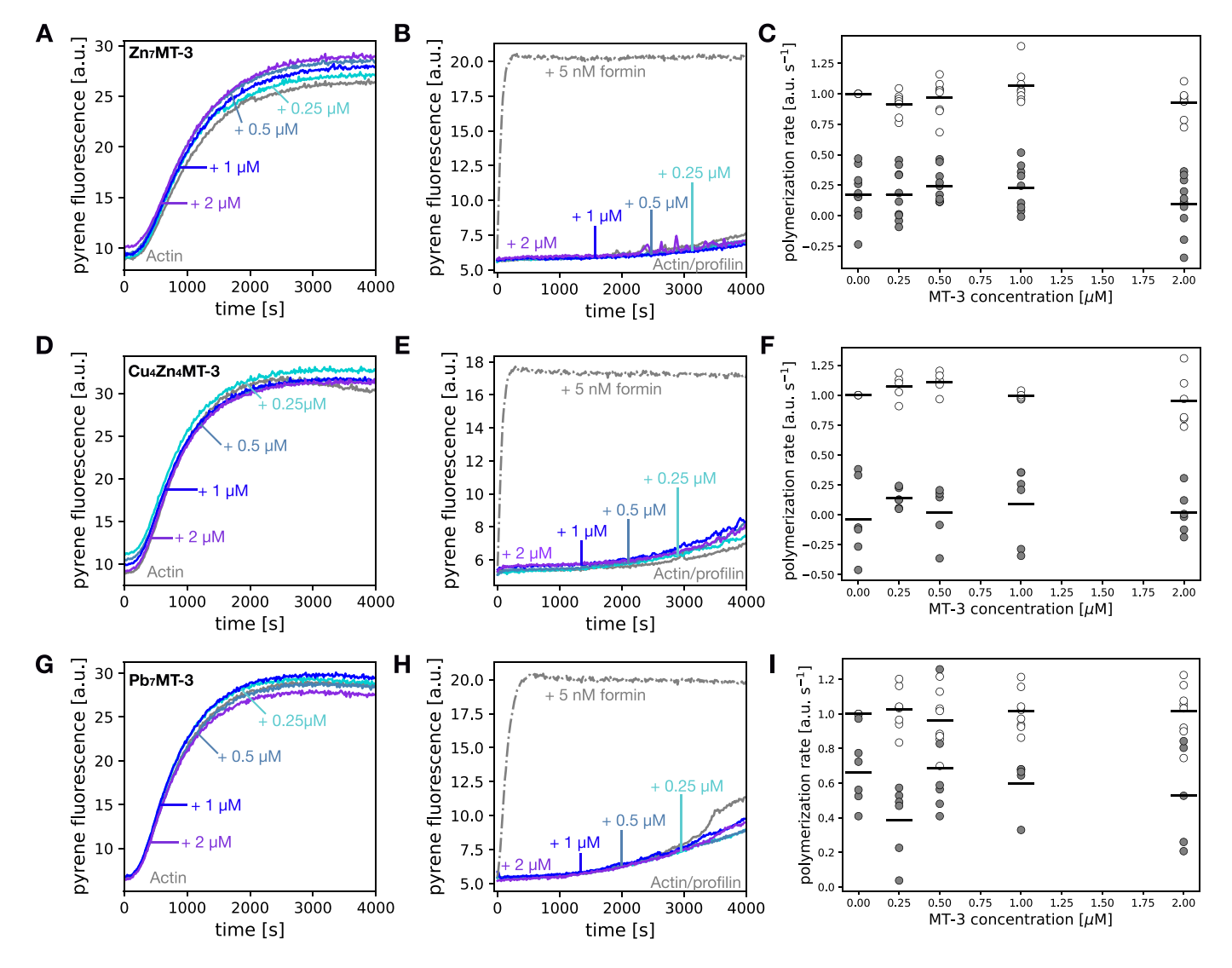


Fig. 5. Recombinant MT-3 does not accelerate actin polymerization. Actin polymerization is not affected by the presence of MT-3 in the (A-C) Zn_7MT -3, (D-F) Cu_4Zn_4MT -3, and (G-I) Pb_7MT -3 forms. Representative raw polymerization traces are shown with varying amounts of MT-3 with either (A, D, F) 4 μ M actin or (B, E, G) 3 μ M actin/6 μ M profilin. For the calculation of polymerization rates (C, F, I), the slope of best fit line at 500 s for 4 μ M actin (open circles) was normalized to the actin alone condition for each experiment. The raw slope values at 1000 s for the profilin/actin condition are plotted (filled circles).

copper transfer to MT-3 alters the MT-3 structure. This assumption is based on the studies of Meloni, Vašák, and coworkers showing that upon mixing Zn₇MT-3 and either Cu²⁺ or Cu²⁺-protein complexes, Zn²⁺ is released and MT-3 reduces four Cu²⁺ to Cu⁺, forming two disulfide bonds in the β domain in the process [38,43]. The coordination geometry and dynamics of the air-stable Cu⁴CysS₅ cluster in the β domain are distinct from the Zn²⁺CysS₉ cluster present in the β domain of Zn₇MT-3 [43]. Further spectroscopic studies would be necessary to confirm that the reaction products of Zn₇MT-3 with Cu²⁺-actin are similar to those reported for other metal swap reactions [37,39,40].

Our results do not support a model of MT-3 as an actin assembly factor on its own. This functional assignment was first proposed in a study by Koh and coworkers, who reported that GFP-MT-3 enhances actin polymerization in the pyrene-actin assay [27]. However, there are key differences in the experimental conditions. Most notably, we used recombinant, bacterially expressed MT-3, and in the earlier study, GFP-MT-3 fusion protein was purified by GFP-immuno-affinity chromatography from mouse astrocytes [27]. These different expression systems lead to at least three important caveats that may provide insight about a putative actin-MT-3 interaction.

First, astrocyte-derived MT-3 could have post-translational modifications (PTMs) that are essential for MT-3 function and are missing in bacterially expressed MT-3. We evaluated one possible PTM, phosphorylation at Ser33, that had been reported in a separate study of MT-3 in cortical neurons [61]. Despite WT-like Zn²⁺ affinity (Fig. S3), the phospho-mimetic variant (S33D) showed a similar lack of stimulation of actin assembly, as found with WT MT-3 (Fig. S4D-F). This does not rule out the possibility of other key PTMs in astrocyte-derived GFP-MT-3. PTMs on actin, most notably lysine acetylation [62], can modulate its interactions with binding proteins. However, rabbit skeletal muscle actin was used in this study and in the experiments of Koh and coworkers [27]. Therefore, actin isoform or modification does not explain the differences we observe in MT-3's stimulation of actin polymerization.

Second, it is possible that GFP-MT-3 from astrocytes co-purifies with an essential binding partner, and together they form a ternary complex with actin. Among the binding partners identified for MT-3 in mass spectrometry screening [25] was dihydropyrimidase-related protein 2 (DRP-2; also known as collapsin response mediator protein 2, CRMP2). DRP-2 promotes axonal growth cone extension [63], and members of the same family have well-characterized, direct effects on actin [64] and

microtubule dynamics [65]. Therefore, DRP-2 is a promising candidate for a cytoskeletal co-regulator that may interact with MT-3 and actin, with the caveat that MT-3 was not identified in a mass spectrometry screen of the DRP-2 interactome [66].

Third, in the earlier study MT-3 was fused to GFP at the N-terminus [27]. The MT-3 used in this study was purified with GFP fused to its N-terminus, and then it was cleaved with TEV protease, leaving an N-terminal Gly-Ser with an unblocked N-terminus. This is distinct from the GFP fusion protein used by Koh and coworkers [27] and also from endogenous MT-3, which is *N*-acetylated at Met1 [17,67]. Therefore, neither this study nor the study of Koh and coworkers [27] capture the most physiologically relevant N-terminus of MT-3. The fact that the N-termini are different in two experiments could point to a role for that region in MT-3-actin interactions, a role supported by data from Koh and co-workers, who show that an N-terminal peptide containing the unique 'TCPCPT' in MT-3 is sufficient to block c-Abl/ F-actin interactions [27].

In addition to a role for MT-3 in astrocyte actin remodeling, MT-3 is implicated in cytoskeletal regulation during the doming of kidney proximal tubule cells [26,68]. The doming process in cultured cells is a model for vectorial active transport. Garrett and coworkers overexpressed V5-tagged MT-3 in HK-2 proximal tubule cells and were able to co-immunoprecipitate β -actin, myosin-9, and enolase 1. Furthermore, MT-3 co-localized with F-actin in the doming HK-2 cell layer [26], and cell lines that did not express MT-3 fail to dome [6,68]. Based on these findings and molecular mechanics docking calculations, Garrett and coworkers proposed a structural model where MT-3 binds to the target-binding cleft of actin between subdomains 1 and 3 via sidechain contacts in the α domain of MT-3. Generally, proteins that bind at this site on actin affect polymerization dynamics, either through filament nucleation, monomer sequestration, barbed end capping, or filament severing [69]. However, none of these activities is observed in our assays. Suppression of actin polymerization due to monomer sequestration or barbed end capping could be observed under conditions in which substantial spontaneous filament nucleation occurs (4 μM actin; Fig. 5A, D, G) but is not seen in the presence of MT-3. Filament nucleation or severing would increase the rate of actin polymerization in a pyrene assay. However, acceleration by MT-3 is not observed in the absence (Fig. 5A, D, G) or presence (Fig. 5B, E, H) of profilin.

In summary, purified, recombinant MT-3 does not bind to muscle actin. The Zn_7MT -3 form of MT-3 removes Cu^{2+} ions from actin filaments, reversing the effects of copper-induced F-actin fragmentation. Zn₇MT-3-mediated Cu²⁺ scavenging has previously been reported from CNS proteins such as amyloid- β , α -synuclein, and prion protein [37,39,40]. These proteins are found in the extracellular compartment, a context where the +2 oxidation state of copper may be more prevalent than in the reducing environment of the cytoplasm, where actin is found [70]. Nonetheless, there are particularly high concentrations of Cu ions in the central nervous system [71], and in cultured neurons, where Cu (of unknown oxidation state) is concentrated at the necks of dendritic spines, a particularly actin-rich structure [35,72]. Actin and microtubules are essential for the structure and stability of dendritic spines [73]. While more research is needed into the role of copper in the brain, the work here suggests that under conditions of Cu²⁺ stress such as those associated with a variety of CNS pathologies [74], actin filaments could be fragmented, altering pre- and post-synaptic structures and therefore learning and memory. MT-3 could scavenge and reduce this copper, reversing the effects of Cu²⁺ on actin networks. Perrin et al. found a delicate balance of actin architecture in the presence of copper: F-actin networks were compromised by excess copper, while copper chelation also decreased F actin content in dendrites [35]. Interestingly, the essential actin severing protein cofilin also binds copper [75], raising the possibility that Cu²⁺ mediates actin structure both directly and via an interaction with cofilin. We posit that understanding the interplay of Cu, MT-3, and the actin cytoskeleton is important to understand MT-3's role as a GIF and generally in the CNS and kidney in health and disease.

Author statement

RL, RNA, CLV: conceptualization, experimental design, data collection and analysis, and manuscript preparation.

CH: conceptualization, experimental design, data collection and analysis.

MRM: experimental design, data collection and analysis, and manuscript preparation.

DEW: experimental design and manuscript preparation.

Declaration of Competing Interest

The authors declare that they have no known competing financial interests or personal relationships that could have appeared to influence the work reported in this paper.

Data availability

Data will be made available on request.

Acknowledgements

The authors are grateful to Naomi Courtemanche for sharing the fascin plasmid and to Jamie Ross and Benjamin Bostick for assistance with ICP-MS. RL, RNA, and CLV were supported by NSF grant CHE-1710176. MRM and DEW were supported by NSF grant CHE-1904705. The microscope was purchased with funds from NSF grant DBI-1828264.

Accession IDs. For recombinant proteins used in this study, the mouse MT-3 amino acid sequence corresponded to UniProt P28184, *S. pombe* profilin to UniProt P39825, and human fascin1 to UniProt Q16658, human DIAPH2 to UniProt O60879-2 (residues 553–1096).

Appendix A. Supplementary data

Supplementary data to this article can be found online at https://doi.org/10.1016/j.jinorgbio.2023.112157.

References

- M. Vašák, D.W. Hasler, Metallothioneins: new functional and structural insights, Curr. Opin. Chem. Biol. 4 (2000) 177–183, https://doi.org/10.1016/S1367-5931 (00)00082-X.
- [2] P. Coyle, J.C. Philcox, L.C. Carey, A.M. Rofe, Metallothionein: the multipurpose protein, CMLS, Cell. Mol. Life Sci. 59 (2002) 627–647, https://doi.org/10.1007/ population.com/article/page/10.1007/ population.com/article/page/
- [3] P. Babula, M. Masarik, V. Adam, T. Eckschlager, M. Stiborova, L. Trnkova, H. Skutkova, I. Provaznik, J. Hubalek, R. Kizek, Mammalian metallothioneins: properties and functions, Metallomics. 4 (2012) 739–750, https://doi.org/ 10.1039/c2mt20081c.
- [4] R.D. Palmiter, S.D. Findley, T.E. Whitmore, D.M. Durnam, MT-III, a brain-specific member of the metallothionein gene family, Proc. Natl. Acad. Sci. U. S. A. 89 (1992) 6333–6337, https://doi.org/10.1073/pnas.89.14.6333.
- [5] B.A. Masters, C.J. Quaife, J.C. Erickson, E.J. Kelly, G.J. Froelick, B.P. Zambrowicz, R.L. Brinster, R.D. Palmiter, Metallothionein III is expressed in neurons that sequester zinc in synaptic vesicles, J. Neurosci. 14 (1994) 5844–5857, https://doi. org/10.1523/JNEUROSCI.14-10-05844.1994.
- [6] S.H. Garrett, M.A. Sens, J.H. Todd, S. Somji, D.A. Sens, Expression of MT-3 protein in the human kidney, Toxicol. Lett. 105 (1999) 207–214, https://doi.org/10.1016/ S0378-4274(99)00003-X.
- [7] V. Günther, U. Lindert, W. Schaffner, The taste of heavy metals: gene regulation by MTF-1, Biochim. Biophys. Acta 2012 (1823) 1416–1425, https://doi.org/10.1016/ i.bbamcr.2012.01.005.
- [8] C.A. Sogawa, M. Asanuma, N. Sogawa, I. Miyazaki, T. Nakanishi, H. Furuta, N. Ogawa, Localization, regulation, and function of metallothionein-III/growth inhibitory factor in the brain, Acta Med. Okayama 55 (2001) 1–9, https://doi.org/ 10.18926/AMO/32031.
- [9] J. Bousleiman, A. Pinsky, S. Ki, A. Su, I. Morozova, S. Kalachikov, A. Wiqas, R. Silver, M. Sever, R.N. Austin, Function of metallothionein-3 in neuronal cells: do metal ions alter expression levels of MT3? Int. J. Mol. Sci. 18 (2017) 1133, https://doi.org/10.3390/jims18061133.
- [10] B. Wang, I.S. Wood, P. Trayhurn, PCR arrays identify metallothionein-3 as a highly hypoxia-inducible gene in human adipocytes, Biochem. Biophys. Res. Commun. 368 (2008) 88–93, https://doi.org/10.1016/j.bbrc.2008.01.036.

- [11] J. He, C. Huang, J. Jiang, L. Lv, Propofol exerts hippocampal neuron protective effects via up-regulation of metallothionein-3, Neurol. Sci. 34 (2013) 165–171, https://doi.org/10.1007/s10072-012-0978-0.
- [12] K.-H. Tsui, C.-P. Hou, K.-S. Chang, Y.-H. Lin, T.-H. Feng, C.-C. Chen, Y.-S. Shin, H.-H. Juang, Metallothionein 3 is a hypoxia-upregulated oncogene enhancing cell invasion and tumorigenesis in human bladder carcinoma cells, Int. J. Mol. Sci. 20 (2019) 980, https://doi.org/10.3390/ijms20040980.
- [13] J.C. Erickson, G. Hollopeter, S.A. Thomas, G.J. Froelick, R.D. Palmiter, Disruption of the metallothionein-III gene in mice: analysis of brain zinc, behavior, and neuron vulnerability to metals, aging, and seizures, J. Neurosci. 17 (1997) 1271–1281, https://doi.org/10.1523/JNEUROSCI.17-04-01271.1997.
- [14] Y. Uchida, Y. Ihara, M. Tomonaga, Alzheimer's disease brain extract stimulates the survival of cerebral cortical neurons from neonatal rats, Biochem. Biophys. Res. Commun. 150 (1988) 1263–1267, https://doi.org/10.1016/0006-291X(88)90765-6
- [15] J.C. Erickson, A.K. Sewell, L.T. Jensen, D.R. Winge, R.D. Palmiter, Enhanced neurotrophic activity in Alzheimer's disease cortex is not associated with downregulation of metallothionein-III (GIF), Brain Res. 649 (1994) 297–304, https:// doi.org/10.1016/0006-8993(94)91076-6
- [16] A.K. Sewell, L.T. Jensen, J.C. Erickson, R.D. Palmiter, D.R. Winge, Bioactivity of metallothionein-3 correlates with its novel β domain sequence rather than metal binding properties, Biochem. 34 (1995) 4740–4747, https://doi.org/10.1021/ bi00014a031
- [17] Y. Uchida, K. Takio, K. Titani, Y. Ihara, M. Tomonaga, The growth inhibitory factor that is deficient in the Alzheimer's disease brain is a 68 amino acid metallothionein-like protein, Neuron. 7 (1991) 337–347, https://doi.org/10.1016/ 0896-6273(91)90272-2.
- [18] W.H. Yu, W.J. Lukiw, C. Bergeron, H.B. Niznik, P.E. Fraser, Metallothionein III is reduced in Alzheimer's disease, Brain Res. 894 (2001) 37–45, https://doi.org/ 10.1016/S0006-8993(00)03196-6.
- [19] A.P. Gunn, C.A. McLean, P.J. Crouch, B.R. Roberts, Quantification of metallothionein-III in brain tissues using liquid chromatography tandem mass spectrometry, Anal. Biochem. 630 (2021), 114326, https://doi.org/10.1016/j. ab.2021.114326.
- [20] Z.-C. Ding, F.-Y. Ni, Z.-X. Huang, Neuronal growth-inhibitory factor (metallothionein-3): structure–function relationships, FEBS J. 277 (2010) 2912–2920, https://doi.org/10.1111/j.1742-4658.2010.07716.x.
- [21] Z.-C. Ding, Q. Zheng, B. Cai, W.-H. Yu, X.-C. Teng, Y. Wang, G.-M. Zhou, H.-M. Wu, H.-Z. Sun, M.-J. Zhang, Z.-X. Huang, Effect of α-domain substitution on the structure, property and function of human neuronal growth inhibitory factor, J. Biol. Inorg. Chem. 12 (2007) 1173–1179, https://doi.org/10.1007/s00775-007-0287-x
- [22] D.W. Hasler, L.T. Jensen, O. Zerbe, D.R. Winge, M. Vašák, Effect of the two conserved prolines of human growth inhibitory factor (metallothionein-3) on its biological activity and structure fluctuation: comparison with a mutant protein, Biochem. 39 (2000) 14567–14575, https://doi.org/10.1021/bi001569f.
- [23] N. Romero-Isart, L.T. Jensen, O. Zerbe, D.R. Winge, M. Vašák, Engineering of metallothionein-3 neuroinhibitory activity into the inactive isoform metallothionein-1, J. Biol. Chem. 277 (2002) 37023–37028, https://doi.org/ 10.1074/jbc.M205730200.
- [24] I. El Ghazi, B.L. Martin, I.M. Armitage, Metallothionein-3 is a component of a multiprotein complex in the mouse brain, Exp. Biol. Med. 231 (2006) 1500–1506, https://doi.org/10.1177/153537020623100908
- [25] I. El Ghazi, B.L. Martin, I.M. Armitage, New proteins found interacting with brain metallothionein-3 are linked to secretion, Int. J. Alzheimers Dis. 2011 (2010), e208634, https://doi.org/10.4061/2011/208634.
- [26] G. Kalyan, A. Slusser-Nore, J.R. Dunlevy, C.S. Bathula, J.B. Shabb, W. Muhonen, S. Somji, D.A. Sens, S.H. Garrett, Protein interactions with metallothionein-3 promote vectorial active transport in human proximal tubular cells, PLoS One 17 (2022), e0267599, https://doi.org/10.1371/journal.pone.0267599.
- [27] S.-J. Lee, K.-S. Cho, H.N. Kim, H.-J. Kim, J.-Y. Koh, Role of zinc metallothionein-3 (ZnMt3) in epidermal growth factor (EGF)-induced c-Abl protein activation and actin polymerization in cultured astrocytes, J. Biol. Chem. 286 (2011) 40847–40856, https://doi.org/10.1074/jbc.M111.245993.
- [28] S.-J. Lee, B.-R. Seo, J.-Y. Koh, Metallothionein-3 modulates the amyloid β endocytosis of astrocytes through its effects on actin polymerization, Mol. Brain. 8 (2015) 84, https://doi.org/10.1186/s13041-015-0173-3.
- [29] B. Roschitzki, M. Vašák, A distinct Cu₄-thiolate cluster of human metallothionein-3 is located in the N-terminal domain, J. Biol. Inorg. Chem. 7 (2002) 611–616, https://doi.org/10.1007/s00775-002-0339-1.
- [30] O. Palacios, S. Atrian, M. Capdevila, Zn- and Cu-thioneins: a functional classification for metallothioneins? J. Biol. Inorg. Chem. 16 (2011) 991–1009, https://doi.org/10.1007/s00775-011-0827-2.
- [31] E. Artells, O. Palacios, M. Capdevila, S. Atrian, In vivo-folded metal-metallothionein 3 complexes reveal the Cu-thionein rather than Zn-thionein character of this brain-specific mammalian metallothionein, FEBS J. 281 (2014) 1659–1678, https://doi.org/10.1111/febs.12731.
- [32] K.P. Kepp, R. Squitti, Copper imbalance in Alzheimer's disease: convergence of the chemistry and the clinic, Coord. Chem. Rev. 397 (2019) 168–187, https://doi.org/ 10.1016/j.ccr.2019.06.018.
- [33] S.S. Lehrer, B. Nagy, J. Gergely, The binding of Cu²⁺ to actin without loss of polymerizability: the involvement of the rapidly reacting -SH group, Arch. Biochem. Biophys. 150 (1972) 164–174, https://doi.org/10.1016/0003-9861(72) 90023-9
- [34] M.R. Mehlenbacher, R. Elsiesy, R. Lakha, R.L.E. Villones, M. Orman, C.L. Vizcarra, G. Meloni, D.E. Wilcox, R.N. Austin, Metal binding and interdomain

- thermodynamics of mammalian metallothionein-3: enthalpically favoured Cu⁺ supplants entropically favoured Zn²⁺ to form Cu[†] clusters under physiological conditions, Chem. Sci. 13 (2022) 5289–5304, https://doi.org/10.1039/D2SC00676E
- [35] L. Perrin, S. Roudeau, A. Carmona, F. Domart, J.D. Petersen, S. Bohic, Y. Yang, P. Cloetens, R. Ortega, Zinc and copper effects on stability of tubulin and actin networks in dendrites and spines of hippocampal neurons, ACS Chem. Neurosci. 8 (2017) 1490–1499, https://doi.org/10.1021/acschemneuro.6b00452.
- [36] J. Gruszczynska-Biegala, A. Stefan, A.A. Kasprzak, P. Dobryszycki, S. Khaitlina, H. Strzelecka-Golaszewska, Myopathy-sensitive G-actin segment 227-235 is involved in salt-induced stabilization of contacts within the actin filament, Int. J. Mol. Sci. 22 (2021) 2327, https://doi.org/10.3390/ijms22052327.
- [37] G. Meloni, V. Sonois, T. Delaine, L. Guilloreau, A. Gillet, J. Teissié, P. Faller, M. Vašák, Metal swap between Zn₇-metallothionein-3 and amyloid-β-Cu protects against amyloid-β toxicity, Nat. Chem. Biol. 4 (2008) 366–372, https://doi.org/ 10.1038/nchembio.89.
- [38] G. Meloni, P. Faller, M. Vašák, Redox silencing of copper in metal-linked neurodegenerative disorders: reaction of Zn₇metallothionein-3 with Cu²⁺ ions, J. Biol. Chem. 282 (2007) 16068–16078, https://doi.org/10.1074/jbc. M701357200.
- [39] G. Meloni, M. Vašák, Redox activity of α-synuclein-Cu is silenced by Zn₇-metallothionein-3, Free Radic. Biol. Med. 50 (2011) 1471–1479, https://doi.org/10.1016/j.freeradbjomed.2011.02.003.
- [40] G. Meloni, A. Crameri, G. Fritz, P. Davies, D.R. Brown, P.M.H. Kroneck, M. Vašák, The catalytic redox activity of prion protein–Cu^{II} is controlled by metal exchange with the Zn^{II}–thiolate clusters of Zn₂metallothionein-3, ChemBioChem. 13 (2012) 1261–1265, https://doi.org/10.1002/cbic.201200198.
- [41] H. Liu, J.H. Naismith, An efficient one-step site-directed deletion, insertion, single and multiple-site plasmid mutagenesis protocol, BMC Biotechnol. 8 (2008) 91, https://doi.org/10.1186/1472-6750-8-91.
- [42] M.C. Carpenter, A. Shami Shah, S. DeSilva, A. Gleaton, A. Su, B. Goundie, M. L. Croteau, M.J. Stevenson, D.E. Wilcox, R.N. Austin, Thermodynamics of Pb(II) and Zn(II) binding to MT-3, a neurologically important metallothionein, Metallomics. 8 (2016) 605–617, https://doi.org/10.1039/c5mt00209e.
- [43] J.S. Calvo, R.L.E. Villones, N.J. York, E. Stefaniak, G.E. Hamilton, A.L. Stelling, W. Bal, B.S. Pierce, G. Meloni, Evidence for a long-lived, Cu-coupled and oxygen-Inert disulfide radical anion in the assembly of metallothionein-3 Cu(I)₄-thiolate cluster, J. Am. Chem. Soc. 144 (2022) 709–722, https://doi.org/10.1021/ iose_1002084
- [44] R. Lakha, A.M. Montero, T. Jabeen, C.C. Costeas, J. Ma, C.L. Vizcarra, Variable autoinhibition among deafness-associated variants of diaphanous 1 (DIAPH1), Biochem. 60 (2021) 2320–2329, https://doi.org/10.1021/acs.biochem.1c00170.
- [45] G. Meloni, M. Knipp, M. Vašák, Detection of neuronal growth inhibitory factor (metallothionein-3) in polyacrylamide gels and by Western blot analysis, J. Biochem. Biophys. Methods 64 (2005) 76–81, https://doi.org/10.1016/j. ibbm.2005.05.005.
- [46] J. Schindelin, I. Arganda-Carreras, E. Frise, V. Kaynig, M. Longair, T. Pietzsch, S. Preibisch, C. Rueden, S. Saalfeld, B. Schmid, J.-Y. Tinevez, D.J. White, V. Hartenstein, K. Eliceiri, P. Tomancak, A. Cardona, Fiji: an open-source platform for biological-image analysis, Nat. Methods 9 (2012) 676–682, https://doi.org/ 10.1038/nmeth.2019.
- [47] M.B. Smith, H. Li, T. Shen, X. Huang, E. Yusuf, D. Vavylonis, Segmentation and tracking of cytoskeletal filaments using open active contours, Cytoskeleton (Hoboken). 67 (2010) 693–705, https://doi.org/10.1002/cm.20481.
- [48] H. Li, T. Shen, M.B. Smith, I. Fujiwara, D. Vavylonis, X. Huang, Automated actin filament segmentation, tracking and tip elongation measurements based on open active contour models, in: 2009 IEEE International Symposium on Biomedical Imaging: From Nano to Macro, 2009, pp. 1302–1305, https://doi.org/10.1109/ ISBL 2009.5193303.
- [49] J.A. Cooper, S.B. Walker, T.D. Pollard, Pyrene actin: documentation of the validity of a sensitive assay for actin polymerization, J. Muscle Res. Cell Motil. 4 (1983) 253–262, https://doi.org/10.1007/BF00712034.
- [50] L.K. Doolittle, M.K. Rosen, S.B. Padrick, Measurement and analysis of in vitro actin polymerization, Methods Mol. Biol. 1046 (2013) 273–293, https://doi.org/ 10.1007/978-1-62703-538-5 16.
- [51] M.L. Pimm, J. Hotaling, J.L. Henty-Ridilla, Profilin choreographs actin and microtubules in cells and cancer, Int. Rev. Cell Mol. Biol. 355 (2020) 155–204, https://doi.org/10.1016/bs.ircmb.2020.05.005.
- [52] K. Hegetschweiler, P. Saltman, Interaction of copper(II) with N-(2-hydroxyethyl) piperazine-N'-ethanesulfonic acid (HEPES), Inorg. Chem. 25 (1986) 107–109, https://doi.org/10.1021/ic00221a028.
- [53] H.E. Mash, Y.-P. Chin, L. Sigg, R. Hari, H. Xue, Complexation of copper by zwitterionic aminosulfonic (good) buffers, Anal. Chem. 75 (2003) 671–677, https://doi.org/10.1021/ac0261101.
- [54] M. Sokołowska, W. Bal, Cu(II) complexation by "non-coordinating" N-2-hydroxyethylpiperazine-N"-2-ethanesulfonic acid (HEPES buffer), J. Inorg. Biochem. 99 (2005) 1653–1660, https://doi.org/10.1016/j.
- [55] T.D. Pollard, Rate constants for the reactions of ATP- and ADP-actin with the ends of actin filaments, J. Cell Biol. 103 (1986) 2747–2754, https://doi.org/10.1083/ ich.1026.2747.
- [56] D.R. Kovar, E.S. Harris, R. Mahaffy, H.N. Higgs, T.D. Pollard, Control of the assembly of ATP- and ADP-actin by formins and profilin, Cell. 124 (2006) 423–435, https://doi.org/10.1016/j.cell.2005.11.038.

- [57] E. Kim, E. Reisler, Intermolecular coupling between loop 38-52 and the C-terminus in actin filaments, Biophys. J. 71 (1996) 1914–1919, https://doi.org/10.1016/ \$0006-3405(96)79390-6
- [58] D. Sept, J. Xu, T.D. Pollard, J.A. McCammon, Annealing accounts for the length of actin filaments formed by spontaneous polymerization, Biophys. J. 77 (1999) 2911–2919, https://doi.org/10.1016/s0006-3495(99)77124-9.
- [59] S. Atrian, M. Capdevila, Metallothionein-protein interactions, Biomol. Concepts. 4 (2013) 143–160, https://doi.org/10.1515/bmc-2012-0049.
- [60] L.J. Jiang, W. Maret, B.L. Vallee, The ATP-metallothionein complex, Proc. Natl. Acad. Sci. U. S. A. 95 (1998) 9146–9149, https://doi.org/10.1073/ pnas.95.16.9146.
- [61] M.A. Aras, H. Hara, K.A. Hartnett, K. Kandler, E. Aizenman, Protein kinase C regulation of neuronal zinc signaling mediates survival during preconditioning, J. Neurochem. 110 (2009) 106–117, https://doi.org/10.1111/j.1471-4159.2009.06106.x.
- [62] A. Mu, T.S. Fung, L.M. Francomacaro, T. Huynh, T. Kotila, Z. Svindrych, H. N. Higgs, Regulation of INF2-mediated actin polymerization through site-specific lysine acetylation of actin itself, Proc. Natl. Acad. Sci. U. S. A. 117 (2020) 439–447, https://doi.org/10.1073/pnas.1914072117.
- [63] N. İnagaki, K. Chihara, N. Arimura, C. Ménager, Y. Kawano, N. Matsuo, T. Nishimura, M. Amano, K. Kaibuchi, CRMP-2 induces axons in cultured hippocampal neurons, Nat. Neurosci. 4 (2001) 781–782, https://doi.org/10.1038/ 90476.
- [64] H.-C. Yu-Kemp, J.P. Kemp, W.M. Brieher, CRMP-1 enhances EVL-mediated actin elongation to build lamellipodia and the actin cortex, J. Cell Biol. 216 (2017) 2463–2479, https://doi.org/10.1083/jcb.201606084.
- [65] Y. Fukata, T.J. Itoh, T. Kimura, C. Ménager, T. Nishimura, T. Shiromizu, H. Watanabe, N. Inagaki, A. Iwamatsu, H. Hotani, K. Kaibuchi, CRMP-2 binds to tubulin heterodimers to promote microtubule assembly, Nat. Cell Biol. 4 (2002) 583–591, https://doi.org/10.1038/ncb825.
- [66] D. Martins-de-Souza, J.S. Cassoli, J.M. Nascimento, K. Hensley, P.C. Guest, A. M. Pinzon-Velasco, C.W. Turck, The protein interactome of collapsin response

- mediator protein-2 (CRMP2/DPYSL2) reveals novel partner proteins in brain tissue, Proteomics Clin. Appl. 9 (2015) 817–831, https://doi.org/10.1002/prca.201500004.
- [67] D.L. Pountney, S.M. Fundel, P. Faller, N.E. Birchler, P. Hunziker, M. Vašák, Isolation, primary structures and metal binding properties of neuronal growth inhibitory factor (GIF) from bovine and equine brain, FEBS Lett. 345 (1994) 193–197, https://doi.org/10.1016/0014-5793(94)00452-8.
- [68] D. Kim, S.H. Garrett, M.A. Sens, S. Somji, D.A. Sens, Metallothionein isoform 3 and proximal tubule vectorial active transport, Kidney Int. 61 (2002) 464–472, https://doi.org/10.1046/j.1523-1755.2002.00153.x.
- [69] R. Dominguez, K.C. Holmes, Actin structure and function, Annu. Rev. Biophys. 40 (2011) 169–186, https://doi.org/10.1146/annurev-biophys-042910-155359.
- [70] M. Siotto, R. Squitti, Copper imbalance in Alzheimer's disease: overview of the exchangeable copper component in plasma and the intriguing role albumin plays, Coord. Chem. Rev. 371 (2018) 86–95, https://doi.org/10.1016/j.ccr.2018.05.020.
- [71] E.L. Que, D.W. Domaille, C.J. Chang, Metals in neurobiology: probing their chemistry and biology with molecular imaging, Chem. Rev. 108 (2008) 1517–1549, https://doi.org/10.1021/cr078203u.
- [72] F. Domart, P. Cloetens, S. Roudeau, A. Carmona, E. Verdier, D. Choquet, R. Ortega, Correlating STED and synchrotron XRF nano-imaging unveils cosegregation of metals and cytoskeleton proteins in dendrites, eLife. 9 (2020), e62334, https://doi. org/10.7554/eLife.62334.
- [73] S. Pelucchi, R. Stringhi, E. Marcello, Dendritic spines in Alzheimer's disease: how the actin cytoskeleton contributes to synaptic failure, Int. J. Mol. Sci. 21 (2020) E908, https://doi.org/10.3390/ijms21030908.
- [74] G. Eskici, P.H. Axelsen, Copper and oxidative stress in the pathogenesis of Alzheimer's disease, Biochem. 51 (2012) 6289–6311, https://doi.org/10.1021/ bi3006169
- [75] S.D. Smith, Y.-M. She, E.A. Roberts, B. Sarkar, Using immobilized metal affinity chromatography, two-dimensional electrophoresis and mass spectrometry to identify hepatocellular proteins with copper-binding ability, J. Proteome Res. 3 (2004) 834–840, https://doi.org/10.1021/pr049941r.